Amine-templated polymeric Mg formates: crystalline scaffolds exhibiting extensive hydrogen bonding

(Article begins on next page)

15 October 2023

Amine-templated polymeric Mg formates: crystalline scaffolds exhibiting extensive hydrogen bonding †

Andrea Rossin,[*a] **Michele R. Chierotti,**[b,c] **Giuliano Giambastiani,**[a] **Roberto Gobetto**[b] **and Maurizio Peruzzini** [*a]

Two novel polymeric Mg formates $[(Fmd)Mg(HCOO)_3]_\infty$ (**1**) and $[(Gua)Mg(HCOO)_3]_\infty$ (**2**) containing the formamidinium $[Fmd^+, (NH_2\text{-}CH^+\text{-}NH_2)]$ and guanidinium $[Gua^+, C^+(NH_2)_3]$ cations have been prepared under solvothermal conditions. **1** and **2** are isostructural; they crystallize in the orthorhombic space group *Pnna*. Their 3D scaffold consists of Mg ions in an octahedral coordination environment bridged by formate ligands. The overall framework charge is negative, and the cations are located in the centre of the lattice cavities, forming extensive N-H⋯O hydrogen bonding with the surrounding cage. Both compounds have been characterized through single-crystal and powder X-ray diffraction, 1D and 2D solid-state NMR (^{1}H, ^{13}C and ^{15}N), IR spectroscopy and TG-MS analysis. Their chemical reactivity towards ion exchange and ability as CO_2 storage materials has been finally examined.

Introduction

The design of crystalline organometallic materials strongly depends on the delicate and non-covalent nature of the intermolecular forces responsible for crystal packing, which often lead to unexpected architectures of the final network obtained in a synthesis.[1] The satisfactory *a priori* prediction of the lowest energy solid-state structure using computational approaches is still the main challenge of contemporary crystal engineering,[2] mainly because of the unpredictable effect of such collective forces. The most diffuse and important example is offered by hydrogen bonding between polar groups.[3] In this respect, amino- and carboxylic groups are almost always involved into robust *charge-assisted* N-H⋯OOC hydrogen bonds.[3] The simultaneous presence of a high number of hydrogen bonds in the structure is an index of its physical and chemical stability. Polyamines often behave as *templates*, assisting the formation of a polycarboxylate network and *vice-versa*,[1c] owing to their ability at forming multiple hydrogen bonds at one time. The creation of a stable 3D structure is frequently observed also in the crystallization of *bifunctional* molecules, *i.e.* species containing both acidic and basic functional groups.[4] Our recent interest in the synthesis of Mg-based light materials for gas storage applications[5] has led to the discovery of two novel polymeric Mg formates, namely $[(Fmd)Mg(HCOO)_3]_\infty$ (**1**) and $[(Gua)Mg(HCOO)_3]_\infty$ (**2**). The negative framework charge is balanced by the presence of the polyamino cations formamidinium $(Fmd^+, NH_2\text{-}CH^+\text{-}NH_2)$ and guanidinium $[Gua^+, C^+(NH_2)_3]$. The ability of Gua^+ to act as a template in the solid-state structure growth is widely described in the literature;[6] on the contrary, the Fmd^+ cation is less investigated; indeed, **1** is only the second example reported in the literature so far besides the zinc(II) analogue[7]

$[(Fmd)Zn(HCOO)_3]_\infty$. The existence of hydrogen bonding between the included amino groups and the formate linkers has been unambiguously demonstrated by both single-crystal X-ray diffraction and ^{1}H CRAMPS and ^{1}H-^{13}C HETCOR NMR analysis. These non-covalent interactions are responsible for both the high thermal stability and the chemical inertness of **1** and **2**.

A useful practical application of these materials could be related to carbon dioxide capture and storage (CCS) technologies,[8] in search for a solution to the ever-growing problem of reducing anthropogenic CO_2 emissions and the related greenhouse effect. The discovery of new materials capable of adsorbing CO_2 reversibly represents one of the biggest challenges of modern materials chemistry. Metal-Organic Frameworks (MOFs) and coordination polymers in general have emerged as a new and promising class of porous adsorbents in the last ten years,[8] due to the huge number of organic ligands and metal ions combinations offering the possibility of a systematic tuning of their pore size. The presence of exposed basic sites in MOFs was found to increase their CO_2 affinity remarkably;[9] thus, both our formates have been tested as CO_2 adsorbents at low temperature (195 K), to assess if the presence of multiple $-NH_2$ groups in the lattice could be useful for carbon dioxide uptake.

Experimental Section

Materials and Methods.

All starting materials and solvents were of analytical grade. They were purchased from Aldrich and used as received, without further purification. Single crystal X-Ray data were collected at low (120 K) or ambient (298 K) temperature for **1** and **2**, respectively, on an Oxford Diffraction XCALIBUR 3

diffractometer equipped with a CCD area detector using Mo K$_\alpha$ radiation (λ = 0.7107 Å). The program used for the data collection was CrysAlis CCD 1.171.[10] Data reduction was carried out with the program CrysAlis RED 1.171[11] and the absorption correction was applied with the program ABSPACK 1.17. Direct methods implemented in Sir97[12] were used to solve the structures and the refinements were performed by full-matrix least-squares against F^2 implemented in SHELX97.[13] All the non-hydrogen atoms were refined anisotropically while the hydrogen atoms of the formate ligands were fixed in calculated positions and refined isotropically with the thermal factor depending on the one of the carbon atom to which they are bound. The Fmd$^+$ and Gua$^+$ N-hydrogens were located on the Fourier difference density maps and refined isotropically with the thermal factor depending on those of the nitrogens to which they are bound. The geometrical calculations were performed by PARST97[14] and molecular plots were produced by the program ORTEP3.[15] X-ray powder diffraction (XRPD) measurements were carried out with a Panalytical X'PERT PRO powder diffractometer equipped with a diffracted beam Ni filter and an PIXcel$^©$ solid state detector in the 4-60° 2θ region, operating with CuK$_\alpha$ radiation (λ = 1.54 Å). Anti-scatter slits were used both on the incident (0.25° and 0.5° divergence) and the diffracted (7.5 mm height) beam. Variable temperature (VT) X-ray powder diffraction patterns were collected in the 25-450 °C temperature range using an Anton Paar HTK 1200N Oven camera. The measurements were carried out at ambient pressure under a mild N$_2$ flow, at a heating rate of 10 °C min^{-1}. Solution ^{11}B NMR spectra were collected on a BRUKER AVANCE II 300 MHz spectrometer (resonance frequency 96.3 MHz). Chemical shifts are reported in parts per million (ppm) and were referenced to BF$_3$· Et$_2$O. Solid-state NMR measurements were run on a Bruker AVANCE II 400 instrument operating at 400.23, 100.65 and 40.56 MHz for ^{1}H, ^{13}C and ^{15}N, respectively. ^{13}C, ^{15}N and 2D spectra were recorded at room temperature at the spinning speed of 12 kHz. Cylindrical 4mm o.d. zirconia rotors with sample volume of 120 mL were employed. For CPMAS experiments, a ramp cross-polarization pulse sequence was used with contact times of 4 ms, a ^{1}H 90° pulse of 2.9 μs, recycle delays of 20 s, and 16-128 (^{13}C) or 2000-3000 (^{15}N) transients. The two pulse phase modulation (TPPM) decoupling scheme was used with a frequency field of 75 kHz. ^{1}H MAS and CRAMPS spectra were acquired in a 2.5 mm probe with a spinning speed of 32 and 12.5 kHz, respectively. MAS spectra were measured using a depth sequence for suppressing the probe background signal. For CRAMPS experiments a wPMLG5 pulse sequence[16] was used with a PMLG pulse of 1.63 μs. 2D ^{1}H-^{13}C HETCOR spectra were measured according to the method of van Rossum *et al.*[17] The proton rf field strength used during the t$_1$ delay for FSLG decoupling and during the acquisition for TPPM decoupling was 82 kHz. Two off-resonance pulses with opposite phases (*i.e.*+x, −x or +y, −y) during the FSLG decoupling were set to 9.96 μs. The contact time was 80 μs. The magic angle (54.78°) pulse length for protons was set at 1.76 μs. Quadrature detection was achieved by using the states-TPPI method. All the data for 64 t$_1$ increments with 56 scans were collected. For the off-resonance CP (LGCP) FSLG-HETCOR NMR the intensity of the B$_1$(^{1}H) field for the CP was 75 kHz with a mixing period of 2.0 ms. The ^{1}H chemical shift

scale in the HETCOR spectra was corrected by a scaling factor of 1/√3 since the ^{1}H chemical-shift dispersion is scaled by a factor of 1/√3 during FSLG decoupling. ^{1}H, ^{13}C and ^{15}N scales were calibrated with adamantane (^{1}H signal at 1.87 ppm), glycine (^{13}C methylene signal at 43.86 ppm) and (NH$_4$)$_2$SO$_4$ (^{15}N signal at 355.8 ppm with respect to CH$_3$NO$_2$) as external standards.

Thermal gravimetric analysis measurements were performed on an EXSTAR Thermo Gravimetric Analyzer (TG/DTA) Seiko 6200 under N$_2$ atmosphere (100 mL min^{-1}). IR spectra were recorded on KBr pellets in the 4000 – 400 cm^{-1} range. Elemental analyses were performed using a Thermo FlashEA 1112 Series CHNS-O elemental analyzer with an accepted tolerance of ± 0.4 units. CO$_2$ adsorption measurements were carried out at 195 K (acetone-dry ice bath) on a Micromeritics ASAP 2020 sorption analyzer. Prior to the measurements, the samples were degassed at 110 °C using a heating rate of 5 °C min^{-1} and holding that temperature for 4 h under dynamic vacuum (10^{-4} torr).

Preparation of [(Fmd)Mg(HCOO)$_3$]$_\infty$ (1).

Magnesium perchlorate hexahydrate Mg(ClO$_4$)$_2$·6H$_2$O (1.84 g, 5.6 mmol) and cyclobutane-1,1′-dicarboxylic acid (0.40 g, 2.8 mmol) were dissolved in 10 mL of formamide. The clear solution was transferred to a Teflon-lined stainless steel autoclave (inner Teflon beaker volume *ca.* 15 mL), sealed and heated under autogeneous pressure at 130 °C for 24 h. After slow overnight cooling, colorless crystals of **1** were collected, washed with ethanol (4 x 10 mL), petroleum ether (4 x 10 mL) and finally dried under a nitrogen stream at room temperature. Yield: 1.034 g (91 %, calculated with respect to the magnesium salt). The phase purity was checked through XRPD, comparing the experimental diffractogram with that calculated from the single-crystal structure (Figure S1). Anal. Calcd. for **1**, C$_4$H$_8$MgN$_2$O$_6$ (204.42): C, 23.50; H, 3.94; N, 13.70. Found: C, 23.64; H, 3.97; N, 13.81. IR bands (KBr, cm^{-1}) for **1**: 3065 m [ν(N-H)]; 2838 m [ν(C-H) formate]; 1730 s and 1618 vs [ν(COO$^-$)]; 1370 s [ν(C-N)], 1320 m, 1081 w, 809 s [γ(C-H)], 748 m, 572 w.

Preparation of [(Gua)Mg(HCOO)$_3$]$_\infty$ (2).

Magnesium perchlorate hexahydrate Mg(ClO$_4$)$_2$·6H$_2$O (0.57 g, 1.7 mmol), cyclobutane-1,1′-dicarboxylic acid (0.50 g, 3.4 mmol) and guanidinium carbonate Gua$_2$CO$_3$ (0.30 g, 1.7 mmol) were dissolved in 10 mL of formamide. Immediate evolution of CO$_2$ was observed. The solution was purged with nitrogen for 10 minutes, in order to entirely remove residual carbon dioxide. The clear solution was transferred to a Teflon-lined stainless steel autoclave (inner Teflon beaker volume *ca.* 15 mL), sealed and heated under autogeneous pressure at 130 °C for 24 h. After slow overnight cooling, colorless crystals of **2** were collected, washed with ethanol (4 x 10 mL), petroleum ether (4 x 10 mL) and finally dried under a nitrogen stream at room temperature. Yield: 0.360 g (95 %, calculated with respect to the magnesium salt). The phase purity was again checked through XRPD (Figure S2). Anal. Calcd. for **2**, C$_4$H$_{10}$MgN$_3$O$_6$ (220.44): C, 21.79; H, 4.57; N, 19.06. Found: C, 21.95; H, 4.29; N, 19.27. IR bands (KBr, cm^{-1}) for **2**: 3165 m [ν(N-H)]; 2848 m [ν(C-H) formate]; 1683 s and 1605 vs [ν(COO$^-$)]; 1369 s [ν(C-N)], 1165 w, 805 s [γ(C-H)], 740 w, 588 w.

Results and discussion

Solvothermal reaction of magnesium(II) salts with an acid of medium strength in amide solvents has been recently exploited by our group for the preparation of polymeric formates,[5] as a result of the acid-catalyzed solvent hydrolysis at high temperature. It is worth noticing that the amide role in the reaction is different when passing from N,N-dimethylformamide (DMF) to the simpler formamide. In fact, while in the former case a simple thermal decomposition takes place, with concomitant formation of the formate anion and dimethylamine, in the latter case an acid-catalyzed condensation between ammonia (deriving from the thermal decomposition of the solvent)[18] and one further molecule of formamide can be reasonably invoked to account for the generation of the formamidinium cation in the network of **1** (Scheme 1). The use of cyclobutane-1,1'-dicarboxylic acid is related to its medium strength (pK_{a1} = 2.92; pK_{a2} = 5.45)[19] that leads to the formation of a *pure* phase, as explained in our previous work on magnesium formates.[5]
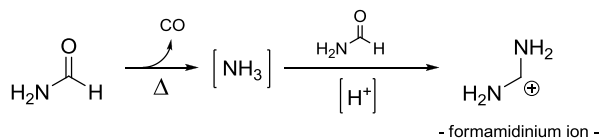
Scheme 1. Generation of the formamidinium ion.

When an "auxiliary" templating cation (like guanidinium) is introduced in solution in the form of Gua$_2$CO$_3$, formation of **2** is more thermodynamically favoured. Reactions with other amine or ammonium salts as templates (urotropine and hydrazine sulphate) were attempted under the same experimental conditions, but they were unsuccessful, probably because of the too large templating size (urotropine) or the template poor thermal stability (hydrazine). In both cases, the final stable product recovered at the end of the synthesis was always **1**.

[(Fmd)Mg(HCOO)$_3$]$_\infty$ crystallizes in the orthorhombic *Pnna* space group; the formate anions are bridging adjacent Mg(II) centers in an octahedral coordination geometry (Figure 1). The metal centre and the Fmd$^+$ C-H bond lie on a mirror plane; therefore, the two N atoms of the cation are symmetry (and magnetically; *vide infra*) equivalent. The 3D scaffold bears a negative charge that is neutralized by Fmd$^+$ in the lattice channels. The –NH$_2$ groups of Fmd$^+$ engage into N-H⋯O hydrogen bonding (N⋯O ~ 2.9 Å) with the surrounding formates, thus providing considerable framework robustness.
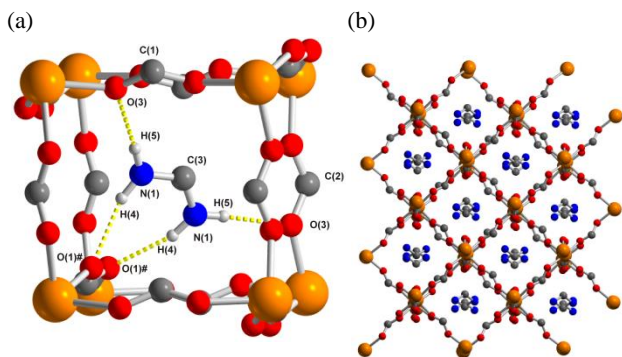
Figure 1. (a) H-bonding network in the crystal structure of **1** and (b) view of the polymer channels along the *c* axis. H atoms on the scaffold omitted for clarity. Atom color code: orange, Mg; gray, C; white, H; red, O; blue, N. Hydrogen bonds depicted in yellow dotted lines.

The main bond distances and angles [d(Mg-O)$_{ave}$ = 2.07 Å; d(C-N) = 1.30 Å; α(O-Mg-O)$_{ave}$ = 90°] fall in the ordinary range observed for other similar species.[20,5] See the Supporting Information for the complete crystallographic data set (Tables S1-S5). The crystal system is identical (and the cell parameters very similar) to that of the Zn(II) analogue [(Fmd)Zn(HCOO)$_3$]$_\infty$ reported by Marsh.[7]

[(Gua)Mg(HCOO)$_3$]$_\infty$ (Figure 2) also crystallizes in the same space group; **1** and **2** are isostructural. The extra-N atom in the cation lies on a mirror plane, and therefore it is also magnetically different from the other two (see NMR below). Refer to the Supporting Information for the complete crystallographic data (Tables S6-S10). Analogously to **1**, extensive N-H⋯O hydrogen bonding (N⋯O ~ 3.0 Å) between Gua$^+$ and the surrounding formate ions is present.
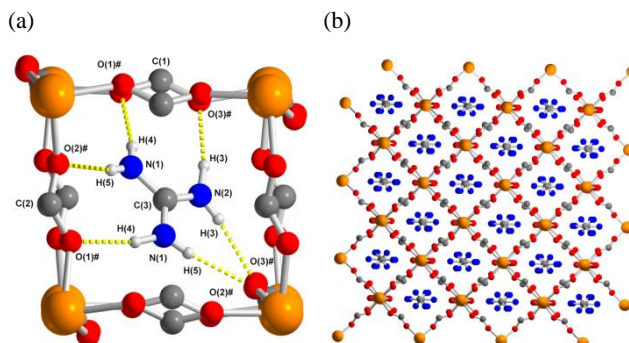
Figure 2. (a) H-bonding network in the crystal structure of **2** and (b) view of the polymer channels along the *c* axis. H atoms on the scaffold omitted for clarity. Atom color code: see Figure 1.

Both **1** and **2** belong to the cubic "pcu" ($4^{12} \cdot 6^3$) network topology,[21] like other perovskite-like related frameworks of general formula [(Cat)M^{II}(HCOO)$_3$]$_\infty$ (Cat = Gua$^+$, NH$_2$Me$_2^+$, MeNH$_3^+$, EtNH$_3^+$, C$_3$H$_8$N$^+$; M = Mn, Fe, Co, Ni, Cu and Zn).[6f,7,22] The templating effect of the protonated amine within the cavities is also evident in the latter cases, and it strongly influences the final crystal lattice topology. In fact, a simple cation change from RNH$_3^+$/R$_2$NH$_2^+$ (R = organic substituent) to ammonium NH$_4^+$ leads to a significant modification of the network type from "pcu" ($4^{12} \cdot 6^3$) to "acs" ($4^9 \cdot 6^6$).[23] At odds with the aforementioned [(Cat)M^{II}(HCOO)$_3$]$_\infty$ systems, in **1** and **2** no guest disorder was found, even at ambient temperature; this implies that within the Magnesium derivatives a *stronger* hydrogen bonding than that observed in their transition metal analogues is present, despite the isostructural nature of the family and the chemical analogy between the divalent cations of the first transition series and the group 2 alkali-earth metals. Another plausible explanation could be related to the presence of (weaker)

C-H···O hydrogen bonding interactions when the guest is of $RNH_3^+/R_2NH_2^+$ type (while they are totally absent in both **1** and **2**).

Additional insights on the H-bonding network in **1** and **2** were gained through solid-state ^1H, ^{13}C and ^{15}N (1D and 2D) NMR spectroscopy. This technique provides complementary information with respect to XRD. In MOF science, solid state NMR spectroscopy is an essential tool for analyzing hydrogen bonding in terms of presence and strength within the network, besides being very useful for the assessment of the guest mobility in the host matrix.[24] In particular, the development of new line narrowing techniques in solids (FSLG or PMLG and DUMBO approaches[25]) are finding increasing applications.[26] ^1H, ^{13}C and ^{15}N chemical shifts with their assignments are reported in Table 3. Proton assignments were deduced from an accurate analysis of the ^1H-^{13}C FSLG HETCOR spectra.

Table 3. ^1H, ^{13}C and ^{15}N chemical shift (ppm) with assignments for compounds **1** and **2**. ^1H assignments were possible only with the help of HETCOR experiments.

compound	^1H	^{13}C	^{15}N
1	9.2 H(5)	175.6 C(1)	84.3
	8.8 H(1)	169.9 C(2)	N(1)/N(2)
	8.4 H(4)	158.6 C(3)	
	8.2 H(2)		
	7.8 H(3)		
2	8.3 H(2)	173.7 C(1)	53.0 N(2)
	8.1 H(1)	171.4 C(2)	48.4 N(1)
	8.0 H(3)/H(4)/H(5)	158.1 C(3)	

Three signals at about 174, 170 and 158 ppm characterize the ^{13}C CPMAS spectra of **1** and **2** (Figure 3). The two high frequency peaks (1:2 ratio) were assigned to the OOC-H carbons of the 3D scaffold, in agreement with three independent formate ligands in the unit cell. Two of them are symmetrical with respect to a mirror plane [C(2)], while the other lies on it [C(1)] (see Figures 1 and 2). Their very narrow line width (36-43 Hz) highlights the high crystallinity of the samples. On the other hand, the low frequency signal assigned to the carbon atom of the cation (158.6 and 158.1 ppm for **1** and **2**, respectively) is broader, because of a residual second-order effect of dipolar coupling to the quadrupolar nitrogen-14 nuclei.[27] Delayed CP experiments (delays 50-100 μs) showed the disappearance of the signal and ruled out broadening effects due to the guest mobility inside the scaffold. This has been further confirmed by the lack of spectral changes in very short contact time CP experiments (contact time = 35-100 μs).

Differences in chemical shifts between **1** and **2** for C(1) and C(2) can be ascribed to the different number and strength of the interactions they are involved in. Indeed, in both **1** and **2** the formate group HC(1)OO is involved into two N-H···O hydrogen bonds with the guest; however, in **1** C(1) shows a high frequency shift (about 2 ppm) generated by the deshielding effect of a further C-H···H-C short contact (H···H distance less than 2.3 Å) with the formamidinium CH group. Similarly, the C(2) peak in **2** is shifted at higher frequency (169.9 ppm in **1** vs. 171.5 ppm in **2**), being involved into only one N-H···O interaction with the guest.
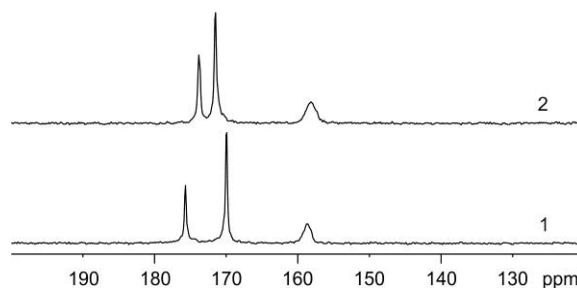

Figure 3. ^{13}C CPMAS spectra of **1** and **2** acquired with a spinning speed of 12 kHz.

The ^{15}N CPMAS spectra (Figure 4) agree with the guest symmetry observed in the X-ray structures: in **1** only one signal at 84.3 ppm could be observed for the two (chemically and magnetically) equivalent nitrogen atoms, while the spectrum of **2** is characterized by two resonances at 53.0 and 48.4 ppm (ratio 1:2) for the nitrogen lying on the mirror plane [N(2)] and the two specular nitrogen atoms [N(1)], respectively.
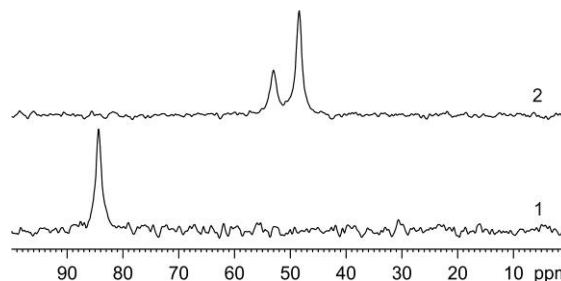

Figure 4. ^{15}N CPMAS spectra of **1** and **2** acquired with a spinning speed of 9 kHz.

The ^1H MAS spectra of **1** and **2** featured only one broad resonance (Figure 5), because of the very strong dipolar coupling. A better resolution is obtained by using the ^1H wPMLG5 pulse sequence;[16] particularly, in the case of **1** an additional shoulder around 9.5 ppm could be resolved. From the shift of the hydrogen-bonded protons, it is clear that the number rather than the strength of the interactions is responsible for the material high stability, because no peak was observed in either the moderate (10-14 ppm) or strong (14-20 ppm) hydrogen bond region.[28] The presence of a plethora of weak interactions is the main reason for the lack of mobility of the guest species.
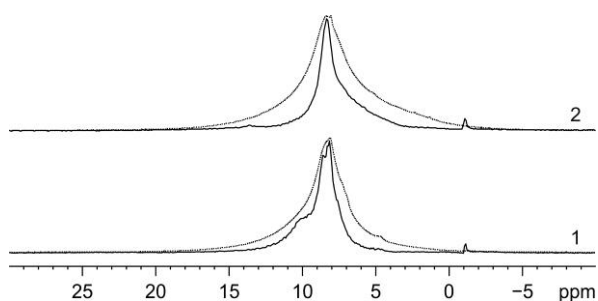
Figure 5. [1]H MAS (dotted lines) and CRAMPS (solid lines) spectra of **1** and **2**. MAS spectra were recorded with a spinning speed of 32 kHz, while CRAMPS spectra were acquired with the *w*PMLG5 sequence at 12.5 kHz.

Additional insights came from the analysis of the [1]H-^{13}C on- and off-resonance CP FSLG HETCOR experiments, allowing for the separation of the chemical shift information into two dimensions and thus overcoming low ^{1}H resolution problems.[29] Proton assignments deduced from the [1]H-^{13}C on-resonance CP FSLG HETCOR are reported in Table 3. The chemical shifts of the guest NH groups could be well defined only through the LGCP HETCOR experiment. In this sequence, the ^{1}H to ^{13}C magnetization transfer relies only on the heteronuclear H-C dipolar interaction avoiding unwanted spin-diffusion effects, since the LG spin-lock effectively averages the strong [1]H-^{1}H homonuclear dipolar interaction.[17] Thus, [1]H-^{13}C spatial proximities up to about 3 Å could be easily monitored.[30] In **1** it was possible to observe correlations between C(3) and three proton signals at about 9.2, 8.4 and 7.8 ppm (Figure 6B). The formers are attributed to H atoms involved in the stronger and weaker N-H···O interactions (N···O distance 2.860 and 2.939 Å), respectively, while the latter is assigned to the proton directly bound to C(3) (already observed in the on-resonance CP HETCOR spectrum, Figure 6A). On the other hand, in **2** C(3) is a quaternary carbon, and the correlations observed on the LGCP HETCOR spectrum are directly related to the N-H signals (Figure 7). Indeed, it was possible to observe a polarization transfer from C(3) to a proton resonance at about 8.0 ppm (with a low frequency shoulder), in line with the presence of slightly weaker N-H···O hydrogen bonds (N···O distances: 3.027, 2.979, and 2.956 Å) than those of **1**.
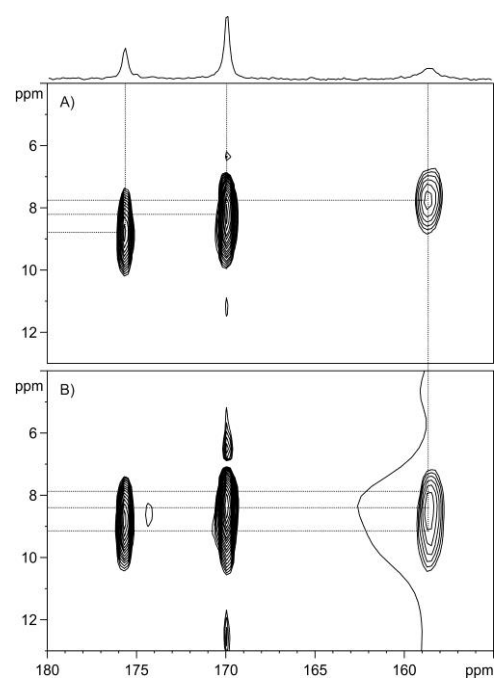

Figure 6. [1]H-^{13}C on-resonance (A) and off-resonance (B) FSLG HETCOR spectra of **1** acquired with a spinning speed of 12 kHz. For the sake of clarity, in B only the slide of the ^{13}C signal at 158.6 ppm has been shown.

Figure 7. [1]H-^{13}C on-resonance (A) and off-resonance (B) FSLG HETCOR spectra of **2** acquired with a spinning speed of 12 kHz. For the sake of clarity, in B only the slide of the ^{13}C signal at 158.1 ppm has been shown.
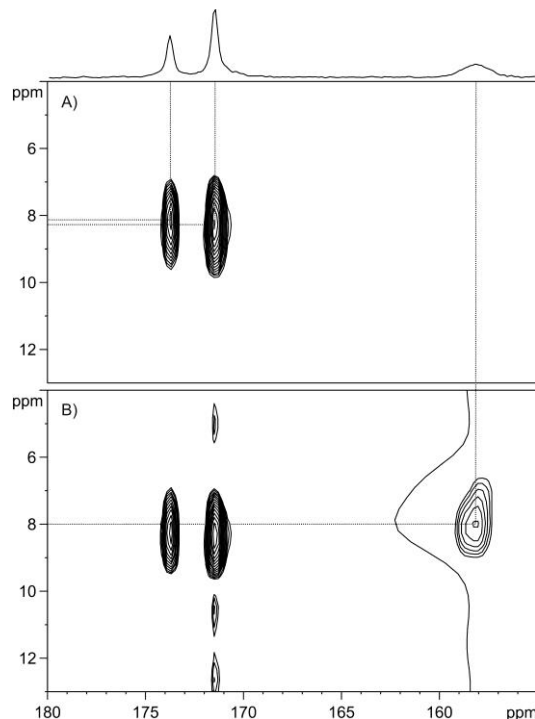
The TG analysis was carried out for both species (Figure 8). Despite the similar structure, their thermal behaviour was found to be significantly different. As already observed in the previously published $H[Mg(HCOO)_3] \supset NHMe_2$ polymer,[5b] in **1** an intermediate (anhydrous) magnesium formate phase was obtained in the 300 – 390 °C temperature range before decomposition (calc. weight loss = 44.1 %). This phase then converts into MgO (calc. weight loss = 36.3 %) above 430 °C$_{onset}$ (also confirmed by the VT-PXRD study; *vide infra*). In **2**, no stable new phase was observed before decomposition occurring at T = 290 °C$_{onset}$; in addition, the onset temperature for the first weight loss in **1** (around 205 °C$_{onset}$) was found to be much lower than that of **2**. This confirms the higher thermal stability of the latter phase, because of the presence of extra hydrogen bonding in the solid-state structure when passing from Fmd$^+$ to Gua$^+$.

stable up to 200 °C, while in the 250 – 400 °C temperature interval the *beta* magnesium formate phase is formed,[31] again in line with what observed during the thermal decomposition of $H[Mg(HCOO)_3] \supset NHMe_2$.[5b] Above 400 °C, the framework collapse generates MgO as final stable product.

Figure 9. VT-XRPD diffractograms of **1** in the 25 – 450 °C temperature range.

Some chemical reactions on **1** were attempted, in order to check if new species could be obtained through a post-synthetic procedure. Prolonged heating (18 h) of a mixture of **1** and calcium borohydride $Ca(BH_4)_2$ in refluxing tetrahydrofuran (thf) only led to a partial cation exchange and concomitant formation of the amino-borane neutral species NH_2-CH_2-$NH_2 \cdot BH_3$ (quartet centered at $\delta_B = -13.0$ ppm, $^1J_{B-H} = 97.4$ Hz),[32] according to the reaction drawn in Scheme 2.

$$[(Fmd)Mg(HCOO)_3] + 0.5\ Ca(BH_4)_2 \longrightarrow [Ca_{0.5}Mg(HCOO)_3] + H_2N\frown NH_2 \cdot BH_3$$
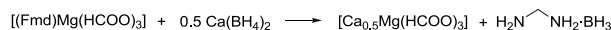
Scheme 2. Reaction of **1** with calcium borohydride.

The reaction never reaches completeness, probably because of the hindered borohydride diffusion into the MOF channels. In addition, the diaminomethane formed after Fmd$^+$ reaction with a hydride source is not stable, and other borane-containing decomposition products were detected on the ^{11}B NMR spectrum of the reaction mixture (Figure S3). According to literature data, they could be identified as ammonia-borane ($NH_3 \cdot BH_3$, quartet centered at $\delta_B = -21.7$ ppm, $^1J_{B-H} = 93.9$ Hz)[33] and methylamine borane ($CH_3NH_2 \cdot BH_3$, quartet centered at $\delta_B = -17.7$ ppm, $^1J_{B-H} = 93.9$ Hz).[33] Reaction with an excess of $BH_3 \cdot thf$ (stoichiometric MOF : borane ratios 1:6 and 1:9 for **1** and **2**, respectively) at ambient temperature for 18 h gave no addition products; only the starting materials were recovered in the end, as confirmed by both XRPD and ^{11}B MAS NMR of the solid residue isolated after workup. The preparation of the "mixed formate" $[LiMg(HCOO)_3]_\infty$ through a cation exchange procedure (Scheme 3) using an excess (10 equiv.) of lithium fluoride (LiF) under hydrothermal conditions (130 °C, 24 h) only provided a mixture of the unreacted reagents.
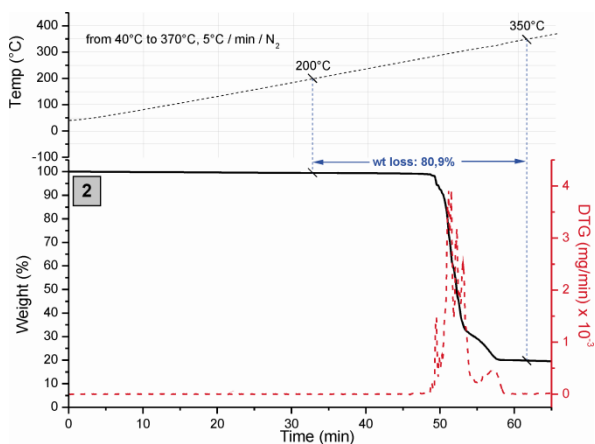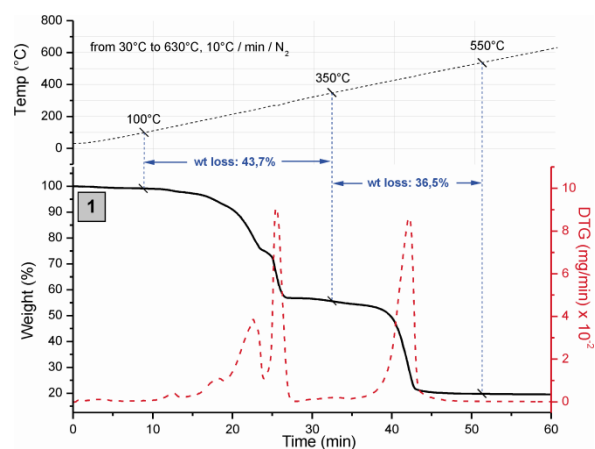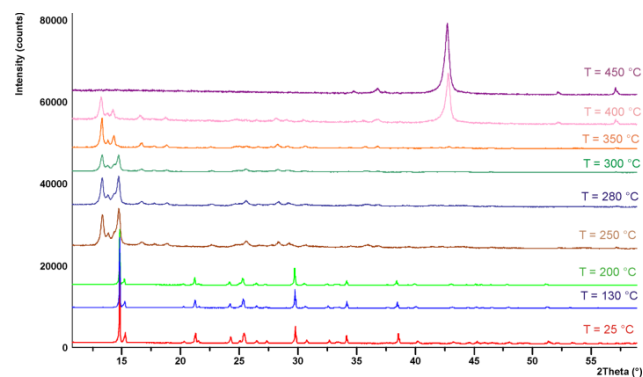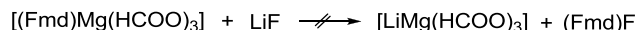

Figure 8. TGA-DTG profiles of **1** and **2**.

The phases identity during the thermal transformation of **1** was assessed through variable-temperature powder X-ray diffraction. The diffractograms collected at increasing temperatures in the 25 – 450 °C range are shown on Figure 9. The initial *Pnna* phase is

$$[(Fmd)Mg(HCOO)_3] + LiF \xrightarrow{\quad\quad} [LiMg(HCOO)_3] + (Fmd)F$$

Scheme 3. Attempted Fmd$^+$ – Li$^+$ cation exchange reaction on **1** using an excess of lithium fluoride.

All the reactions described above highlight the uncommon chemical stability of these salts, probably owing to the strong lattice energy provided by the high number of host-guest hydrogen bonds that "block" the guest into the scaffold channels and make it rather unreactive.

In search for possible practical applications of the materials synthesized, their CO_2 sorption capacities were finally determined through carbon dioxide physisorption at low temperature (195 K) and ambient pressure (760 torr, Figure S4). The adsorption isotherm of **1** shows a maximum uptake value of 0.36 cm^3/g (or $\approx$ 0.1 wt.%). In the case of **2**, a similar behaviour was observed, with a maximum CO_2 uptake of 0.32 cm^3/g (or $\approx$ 0.1 wt.%). The quantities obtained do not seem to depend on the number of –NH$_2$ groups present in the salt; the amount of gas adsorbed is much lower than those reported for other polymeric porous formate materials, both at ambient (between 1.36 and 8.8 wt.% at T = 298 K)[34,5a] and low (20 wt.% at T = 195 K)[35] temperatures. This is probably due to a limited CO_2 pore access, the diffusion being hindered by the cations in the channels. In line with this hypothesis, the sorption capacity of **1** (where the cation is *smaller* in size) is slightly higher than that of **2** (with a *larger* guest in the channels), at any p/p^0 value considered. In addition, the N$_2$ adsorption isotherms recorded for both samples at 77 K and the related BET analysis gave no inner suface area, the materials being non porous.

Conclusions

In summary, two novel polymeric Mg formates built-up around polyamino cations as templating agents have been prepared and completely characterized. The compounds are isostructural: the bridging [Mg-OC(H)O-Mg] motif gives rise to a 3D network sustained by extensive N-H···O hydrogen bonding between the embedded counterion and the surrounding cage. The simultaneous presence of many weak interactions gives these materials a significant thermal and chemical stability. Solid-state NMR analysis has provided evidence for hydrogen bond strengths in both **1** and **2**. By combining ^{1}H CRAMPS and 2D ^{1}H-^{13}C LGCP FSLG HETCOR data it has been inferred that the number rather than the strength of the interactions are responsible of the strong stability of the host-guest systems. Finally, their CO_2 sorption capacity has been assessed at 195 K and p = 760 torr; a light-weight, abundant and non-toxic metal like magnesium is the ideal constituent of attractive "sponges" for practical gas storage applications, especially for portable devices (where the tank weight is of fundamental importance). With this in mind, further experiments are in progress in our laboratories with the aim of synthesizing new porous Mg-based materials.

Notes and references

^{a} *Consiglio Nazionale delle Ricerche, Istituto di Chimica dei Composti Organometallici (ICCOM-CNR), Via Madonna del Piano 10, 50019 Sesto Fiorentino (Firenze), Italy.; E-mail: a.rossin@iccom.cnr.it*
^{b} *Dipartimento di Chimica IFM, Università di Torino, V. Giuria 7, 10125 (Torino), Italy.*
^{c} *NIS Centre of Excellence, Via Quarello 11, 10135 Torino, Italy.*

1 (a) G. M. Schmidt, J. *Pure Appl. Chem.* 1971, **27**, 647-678. (b) G. R. Desiraju, *Crystal Engineering: The Design of Organic Solids*, Elsevier New York (1989), and references therein. (c) G. R. Desiraju, *Crystal Design: Structure and Function* (volume 7), John Wiley & Sons (2003), and references therein.

2 (a) J. D. Dunitz, *Chem. Commun.* 2003, 545-548. (b) J. D. Dunitz, A. Gavezzotti, *Angew. Chem. Int. Ed.* 2005, **44**, 1766-1787.

3 (a) M. C. Etter, *Acc. Chem. Res.* 1990, **23**, 120-126. (b) J. Bernstein, M. C. Etter, L. Leiserowitz, in *Structure and Correlation*, VCH (1994).

4 (a) M. Mitzutani, N. Maejima, K. Jitsukawa, H. Masuda, H. Einaga, *Inorg. Chim. Acta* 1998, **283**, 105-110. (b) J. Weng, M. Hong, Q. Shi, R. Cao, A. S. C. Chan, *Eur. J. Inorg. Chem.* 2002, 2553-2556. (c) L. E. Gordon, W. T. A. Harrison, *Inorg. Chem.* 2004, **43**, 1808-1809. (d) E. V. Anokhina, A. J. Jacobson, *J. Am. Chem. Soc.* 2004, **126**, 3044-3045. (e) J. Fan, C. Slebodnik, R. Angel, B. E. Hanson, *Inorg. Chem.* 2005, **44**, 552-558. (f) L. Chen, X. Bu, *Chem. Mater.* 2006, **18**, 1857-1860. (g) A. Rossin, B. Di Credico, G. Giambastiani, L. Gonsalvi, M. Peruzzini, G. Reginato, *Eur. J. Inorg. Chem.* 2011, 539-548.

5 (a) A. Rossin, A. Ienco, F. Costantino, T. Montini, B. Di Credico, M. Caporali, L. Gonsalvi, P. Fornasiero, M. Peruzzini *Cryst. Growth Des.* 2008, **8**, 3302-3308. (b) A. Rossin, D. Fairen-Jimenez, T. Düren, G. Giambastiani, M. Peruzzini, G. J. Vitillo, *Langmuir* 2011, **27**, 10124-10131.

6 (a) V. A. Russell, C. C. Evans, W. Li, M. D. Ward, *Science* 1997, **276**, 575-579. (b) P. Shiv Halasyamani, R. P. Francis, S. M. Walker, D. O'Hare, *Inorg. Chem.* 1999, **38**, 271-279. (c) W. T. A. Harrison, M. L. F. Phillips, J. Stanchfield, T. M. Nenoff, *Angew. Chem. Int. Ed.* 2000, **39**, 3808-3810. (d) B. F. Abrahams, M. G. Haywood, R. Robson, *J. Am. Chem. Soc.* 2005, **127**, 816-817. (e) J. Han, C.-W. Yan, C.-K. Lam, T. C. W. Mak, *J. Am. Chem. Soc.* 2008, **130**, 10315-10326. (f) K.-L. Hu, M. Kurmoo, Z. Wang, S. Gao, *Chem. Eur. J.* 2009, **15**, 12050-12064. (g) A. C. Soegiarto, A. Comotti, M. D. Ward, J. *Am. Chem. Soc.* 2010, **132**, 14603-14616. (h) S. Reinoso, B. S. Bassil, M. Baruskova, U. Kortz, *Eur. J. Inorg. Chem.* 2010, **17**, 2537-2542.

7 R. E. Marsh, *Acta Cryst. C* 1986, **C42**, 1327-1328.

8 (a) S. Choi, J. H. Drese, C. W. Jones, *ChemSusChem* 2009, **2**, 796-854, and references cited therein. (b) J.-R. Li, Y. Ma, M. C. McCarthy, J. Sculley, J. Yu, H.-K. Jeong, P. B. Balbuena, H.-C. Zhou, *Coord. Chem. Rev.* 2011, **255**, 1791-1823, and references cited therein.

9 (a) S. Couk, J. F. M. Denayer, G. V. Baron, T. Rémy, J. Gascon, F. Kapteijn, *J. Am. Chem. Soc.* 2009, **131**, 6326-6327. (b) A. Demessence, D. M. D'Alessandro, M. L. Foo, J. R. Long, *J. Am. Chem. Soc.* 2009, **131**, 8784-8786. (c) B. Zheng, J. Bai, J. Duan, L. Wojtas, M. J. Zaworotko, *J. Am. Chem. Soc.* 2011, **133**, 748-751.

10 *CrysAlisCCD 1.171.31.2* (release 07-07-2006), CrysAlis171 .NET, Oxford Diffraction Ltd.

11 *CrysAlis RED 1.171.31.2* (release 07-07-2006), CrysAlis171 .NET, Oxford Diffraction Ltd.

12 A. Altomare, M. C. Burla, M. Camalli, G. L. Cascarano, C. Giacovazzo, A. Guagliardi, A. G. G. Moliterni, G. Polidori, R. Spagna, *J. Appl. Crystallogr.* 1999, **32**, 115-119.

13 G. M. Sheldrick, *SHELXL* (1997).

14 M. Nardelli, *Comput. Chem.* 1993, **7**, 95-98.

15 L. J. Farrugia, *J. Appl. Crystallogr.* 1997, **30**, 565.

16 E. Vinogradov, P. K. Madhu, S. Vega, *Chem. Phys. Lett.* 2002, **354**, 193–202.

17 B. J.; van Rossum, C. P. de Groot, V. Ladizhansky, S. Vega, H. J. M. de Groot, *J. Am. Chem. Soc.* 2000, **122**, 3465-3472.

18 (a) V. S. Nguyen, H. L. Abbott, M. M. Dawley, T. M. Orlando, J. Leszczynski, M. T. Nguyen, *J. Phys. Chem. A* 2011, **115**, 841-851. (b) R. A. Back, J. C. Boden, *Trans. Faraday Soc.* 1971, **67**, 88-96.

19 R. Cali, S. Gurrieri, E. Rizzarelli, S. Sammartano, *Thermochimica Acta* 1975, **12**, 19-23.

20 (a) J. P. Beale, J. A. Cunningham, D. J. Phillips, *Inorg. Chim. Acta* 1979, **33**, 113-118. (b) S. Parola, R. Khem, D. Cornu, F. Chassegneux, S. Lecocq, Z. Kighelman, N. Setter, *Inorg. Chem. Commun.* 2002, **5**, 316-318. (c) R.-J. Tao, C.-Z. Mei, B.-T. Liu, *Chin. J. Chem.* 2006, **24**, 1559-1563. (d) B. Courcot, D. Firley, B. Fraisse, P. Becker, J.-M. Gillet, P. Pattison, D. Chernyshov, M. Sghaier, F. Zouhiri, D. Desmaele, J. D'Angelo, F. Bonhomme, S. Geiger, N. E. Ghermani, *J. Phys. Chem. B* 2007, **111**, 6042-6050.

21 M. O'Keeffe, M. A. Peskov, S. J. Ramsden, O. M. Yaghi, *Acc. Chem. Res.* 2008, **41**, 1782-1789.

22 (a) Z. Wang, K. Hu, S. Gao, H. Kobayashi, *Adv. Mater.* 2010, **22**, 1526-1533. (b) P. Jain, V. Ramachandran, R. J. Clark, H. D. Zhou, B. H. Toby, N. S. Dalal, H. W. Kroto, A. K. Cheetham, *J. Am. Chem. Soc.* 2009, **131**, 13625-13627. (c) P. Jain, N. S. Dalal, B. H. Toby, H. W. Kroto, A. K. Cheetham, *J. Am. Chem. Soc.* 2008, **130**, 10450-10451. (d) Z. Wang, B. Zhang, T. Otsuka, K. Inoue, H. Kobayashi, M. Kurmoo, *Dalton Trans.* 2004, 2209-2216.

23 (a) G.-C. Xu, W. Zhang, X.-M. Ma, Y.-H. Chen, L. Zhang, H.-L. Cai, Z.-M. Wang, R.-G. Xiong, S. Gao, *J. Am. Chem. Soc.* 2011, **133**, 14948-14951. (b) G.-C. Xu, X.-M. Ma, L. Zhang, Z.-M. Wang, S. Gao, *J. Am. Chem. Soc.* 2010, **132**, 9588-9590. (c) Z. Wang, B. Zhang, K. Inoue, H. Fujiwara, T. Otsuka, H. Kobayashi, M. Kurmoo, *Inorg. Chem.* 2007, **46**, 437-445.

24 M. R. Chierotti, R. Gobetto, *Eur. J. Inorg. Chem.* 2009, 2581-2597.

25 S. P. Brown, *Solid State Nucl. Magn. Reson.* 2012, **41**, 1-27.

26 (a) F. Gul-E-Noor, B. Jee, A. Poppl, M. Hartmann, D. Himsl, M. Bertmer, *Phys. Chem. Chem. Phys.* 2011, **13**, 7783-7788. (b) C. Lieder, S. Opelt, M. Dyballa, H. Henning, E. Klemm, M. Hunger, *J. Phys. Chem. C* 2010, **114**, 16596-16602. (c) G. Maruta, S. Takeda, *Polyhedron* 2005, **24**, 16-17.

27 (a) R. K. Harris, A. C. Olivieri, *Prog. Nucl. Magn. Reson. Spectrosc.* 1992, **24**, 435-456. (b) R. Gobetto, C. Nervi, E. Valfrè, M. R. Chierotti, D. Braga, L. Maini, F. Grepioni, R. K. Harris, P. Y. Ghi, *Chem. Mater.* 2005, **17**, 1457-1466.

28 (a) M. R. Chierotti, R. Gobetto, *Chem. Commun.* 2008, 1621-1634. (b) M. R. Chierotti, L. Ferrero, N. Garino, R. Gobetto, L. Pellegrino D. Braga, F. Grepioni, L. Maini, *Chem. Eur. J.* 2010, **16**, 4347-4358.

29 M. J. Duer, "*Solid-state NMR spectroscopy: principles and applications*" Wiley-Blackwell, (2002).

30 R. Bettini, R. Menabeni, R. Tozzi, M. B. Pranzo, I. Pasquali, M. R. Chierotti, R. Gobetto, L. Pellegrino, *J. Pharm. Sci.* 2010, **99**, 1855-1870.

31 A. K. Powell, C. E. Anson, M. Viertelhaus, *Z. Anorg. Allg. Chem.* 2005, **631**, 2365-2370.

32 The assignment of the ^{11}B NMR peak was made by performing the reaction between methylenediamine dihydrochloride (NH_2-CH_2-NH_2·2HCl) and calcium borohydride under the same experimental conditions. Hydrogen evolution was observed, together with *the same products as those observed in the reaction with* **1** on the ^{11}B NMR spectrum. All of them contain *sp^3*-hybridized boron atoms as BH_3 (quartets). Attempts to isolate single crystals of NH_2-CH_2-NH_2·BH_3 from a THF/*n*-pentane solution mixture at low temperature (− 30 °C) failed.

33 (a) C. Gervais, F. Babonneau, J. Maquet, C. Bonhomme, D. Massiot, E. Framery, M. Vaultier, *Magn. Res. Chem.* 1998, **36**, 407-414. (b) M. E. Bowden, I. W. M. Brown, G. J. Gainsford, H. Wong, *Inorg. Chim. Acta* 2008, **361**, 2147-2153.

34 (a) D. G. Samsonenko, H. Kim, Y. Sun, G.-H. Kim, H.-S. Lee, K. Kim, *Chem. Asian J.* 2007, **2**, 484-488. (b) A. Mallick, S. Saha, P. Pachfule, S. Roy, R. Banerjee, *Inorg. Chem.* 2011, **50**, 1392-1401.

35 D. N. Dybstev, H. Chun, S.-H. Yoon, D. Kim, K. Kim, *J. Am. Chem. Soc.* 2004, **126,** 32-33.